Site-directed RNA repair of endogenous Mecp2 RNA in neurons

John R. Sinnamon[a,1], Susan Y. Kim[a,1], Glen M. Corson[a], Zhen Song[b], Hiroyuki Nakai[b], John P. Adelman[a], and Gail Mandel[a,2]

[a]Vollum Institute, Oregon Health and Science University, Portland, OR 97239; and [b]Department of Molecular and Medical Genetics, Oregon Health and Science University, Portland, OR 97239

Contributed by Gail Mandel, September 22, 2017 (sent for review August 30, 2017; reviewed by Gordon G. Carmichael and Stuart Cobb)

Rett syndrome (RTT) is a debilitating neurological disorder caused by mutations in the gene encoding the transcription factor Methyl CpG Binding Protein 2 (MECP2). A distinct disorder results from *MECP2* gene duplication, suggesting that therapeutic approaches must restore close to normal levels of MECP2. Here, we apply the approach of site-directed RNA editing to repair, at the mRNA level, a disease-causing guanosine to adenosine (G > A) mutation in the mouse MeCP2 DNA binding domain. To mediate repair, we exploit the catalytic domain of Adenosine Deaminase Acting on RNA (ADAR2) that deaminates A to inosine (I) residues that are subsequently translated as G. We fuse the ADAR2 domain, tagged with a nuclear localization signal, to an RNA binding peptide from bacteriophage lambda. In cultured neurons from mice that harbor an RTT patient G > A mutation and express engineered ADAR2, along with an appropriate RNA guide to target the enzyme, 72% of *Mecp2* mRNA is repaired. Levels of MeCP2 protein are also increased significantly. Importantly, as in wild-type neurons, the repaired MeCP2 protein is enriched in heterochromatic foci, reflecting restoration of normal MeCP2 binding to methylated DNA. This successful use of site-directed RNA editing to repair an endogenous mRNA and restore protein function opens the door to future in vivo applications to treat RTT and other diseases.

RNA editing | MeCP2 | Rett syndrome | ADAR2

Rett syndrome (RTT) is a neurodevelopmental disorder due to sporadic mutations in the transcription factor, Methyl CpG Binding Protein 2 (*MECP2*) (1). *MECP2* is located on the X chromosome. Because of dosage compensation mechanisms in mammals, females affected with RTT are mosaic, with an ∼50:50 split between wild-type and mutant cells. Females with *MECP2* mutations undergo regression of early developmental milestones, such as speech and purposeful hand motions, and then acquire severe motor abnormalities, including respiration, and die on average by age 40 (2, 3). Males with mutations in *MECP2*, with a single X chromosome, have an even more profound disease, usually succumbing before 2 y of age (4). There is no cure for RTT.

Mice engineered with mutations in *Mecp2* that cause RTT in humans, either germ line or confined to neural cells, exhibit growth abnormalities, anxiety, and motor deficits, which are similar to RTT patients (5–7). Studies in mice indicate that the most robust RTT phenotypes are neurological, affecting both neurons and glia (6, 8), although many other tissues are also likely affected (9). As in humans, male Rett mice have a more severe disease than female mice. For example, female Rett mice live a normal lifespan, while male mice die between 3 and 4 mo of age (5, 7). At the cellular level, neural cells in Rett male and female mice have smaller somas, nuclei, and reduced process complexities (10–16), reminiscent of affected human cells (17–20). Importantly, restoration of MeCP2 in *Mecp2*-null mice, via conditional Cre recombinase (21) or gene therapy approaches (22–25), reverses many of the Rett-like symptoms and cellular deficits, even in late stages of the disease. The phenotype reversals suggest that in humans, RTT may be amenable to gene replacement strategies (14, 22–25). However, duplications spanning the *MECP2* gene in humans result in MECP2 overexpression and a severe neurological disorder (26). Further, MeCP2 in mice is expressed to different levels in different neural cell types, and perhaps as a consequence, loss of MeCP2 function in mice results in cell-specific alterations in gene expression (27–31). These findings underscore the challenges for *MECP2* gene replacement that must be finely tuned to restore normal MECP2 levels and cellular physiology across diverse cell types in the nervous system. We hypothesized that repairing *MECP2* mutations at the level of mRNA could circumvent the problems of both MECP2 overexpression and cell type-specific regulation.

To test this hypothesis, we targeted guanosine to adenosine (G > A) mutations that underlie RTT (32). We selected this group of mutations as a starting point because there is a family of naturally occurring enzymes, Adenosine Deaminase Acting on RNA (ADAR), which hydrolytically deaminates A to inosine (I) (33–37) in endogenous mRNAs. I base pairs with cytosine (C) and is translated by the ribosome as G (38). One ADAR family member, ADAR2, is expressed to high levels in brain where it posttranscriptionally alters protein functions, such as ion channel permeability, through deamination of the primary transcript (39–41). In addition to its catalytic activity, natural editing by ADAR2 requires recognition of a double-stranded RNA structure, mediated by an intron in the pre-mRNA, which appropriately positions the target A in an exon for editing (39, 42–46). Similar to strategies

Significance

Rett syndrome (RTT) is a neurological disease caused by mutations in the gene encoding the global transcriptional regulator, Methyl CpG Binding Protein 2 (MECP2). We exploit a strategy to repair mutant *Mecp2* mRNA that if successful should reverse symptoms. The strategy utilizes the catalytic activity of a naturally occurring enzyme, Adenosine Deaminase Acting on RNA (ADAR2), which in brain alters the mRNA sequence and function of proteins. In cultured RTT neurons co-expressing a modified ADAR2 protein and an appropriate RNA guide, a human mutation in *Mecp2* mRNA is repaired efficiently. RNA repair restores MeCP2 function, consistent with reversal of the pathological consequences of the RTT mutation. Our strategy holds promise for new therapeutic approaches to RTT and other neurological diseases.

Author contributions: J.R.S., S.Y.K., G.M.C., H.N., J.P.A., and G.M. designed research; J.R.S., S.Y.K., G.M.C., and Z.S. performed research; H.N. contributed new reagents/analytic tools; J.R.S., S.Y.K., G.M.C., J.P.A., and G.M. analyzed data; and J.R.S., J.P.A., and G.M. wrote the paper.

Reviewers: G.G.C., University of Connecticut Health Center; and S.C., University of Glasgow.

The authors declare no conflict of interest.

[1]J.R.S. and S.Y.K. contributed equally to this work.

[2]To whom correspondence should be addressed. Email: mandelg@ohsu.edu.

This article contains supporting information online at www.pnas.org/lookup/suppl/doi:10.1073/pnas.1715320114/-/DCSupplemental.

used to exploit functional domains in other modular enzymes, a cloned catalytic domain in human ADAR2 (hADAR2) has been harnessed, in various configurations, to target G > A repair in heterologously expressed mRNAs, usually at stop codons (47–52). In one approach, replicated in our present study, the native RNA binding domains in ADAR2 are replaced with an RNA binding peptide from bacteriophage lambda (λN, ref. 52) that binds to a specific short RNA hairpin with nanomolar affinity (53). Targeted editing of heterologous mRNA is then achieved by expression of the hybrid ADAR2 protein along with an RNA guide that contains the λN-recognized stem loops and a region complementary to the target mRNA (51, 52).

No endogenous mRNAs have been repaired by site-directed RNA editing. Nonetheless, we were encouraged to test this approach for G > A mutations in endogenous *Mecp2*. First, the mutations in *Mecp2* are in domains that encode well-established functions. Second, the fidelity of repair can be monitored by sequence analysis, Western blotting, and at the single cell level, immunochemistry. Here, we exploit the recombinant hADAR2-λN protein (hereafter, Editase) to test for effective repair of G > A mutations within endogenous *Mecp2* transcripts. After determining parameters for *Mecp2* editing in transfected mouse neuroblastoma (N2A) cells, we use adeno-associated virus (AAV) to transduce primary neuronal cultures from a RTT mouse model that contains a severe human G > A mutation in the DNA binding domain ($MeCP2^{R106Q}$). This mutation results in reduced MeCP2 protein levels and greatly attenuated binding to heterochromatin. We first quantitate editing efficiency of the mutant mRNA in neurons and then test whether editing rescues MeCP2 protein levels and leads to enrichment of binding in heterochromatin foci, a key property of MeCP2 in mouse neurons. Our results show that site-directed RNA editing holds therapeutic promise for repairing disease-causing *MECP2* mutations underlying RTT as well as other neurological diseases amenable to gene therapy.

Results

Targeting Editase to Heterologously Expressed *Mecp2* mRNA Can Repair *Mecp2* G > A Mutations. There are at least three G > A mutations in human *MECP2* that give rise to classical RTT. Two mutations reside within the Methyl DNA Binding Domain (MBD), $MeCP2^{R106Q}$ and $MeCP2^{W104X}$, and one, $MeCP2^{R306H}$, resides in the NCoR interaction domain (NID) (32, 54) (Fig. 1*A*). To determine whether Editase could repair these mutations, we first tested editing following transient transfections of Editase, guide RNA, and *Mecp2* cDNAs into N2A cells. To distinguish heterologously expressed MeCP2 proteins from endogenous ones, the heterologously expressed MeCP2 was tagged with C-terminal eGFP (see *Materials and Methods*). Editase and *Mecp2-gfp* cDNAs were expressed from the cytomegalovirus (CMV) immediate early gene promoter-enhancer, and guide was expressed from the human U6 small nuclear RNA gene promoter. Three copies of the Simian virus 40 large T antigen nuclear localization signal (NLS) were added to the Editase, in addition to the λN peptide, because ADAR2 edits endogenous mRNAs in the nucleus as a primary transcript (55). Each guide RNA contains two stem loops (BoxB) representing the sequences recognized by the λN peptide. One BoxB stem loop is located 16–18 bases 5′ of the target A, and the second is located 10 bases 3′ of the target A (Fig. 1*B*). The number and position of the stem loops relative to the target A were based on previous studies (51, 52) and determined empirically by us for *Mecp2* in transfection analyses before this study. Editing is optimal with a C mismatch at that site in the complementary guide (50, 56, 57), and all *Mecp2* guide mRNAs contain this mismatch.

The N2A cells were cotransfected with separate plasmids encoding Editase, MeCP2-GFP, and a third plasmid either containing or lacking the guide sequences. After 3 d, we used Sanger sequencing to analyze cDNAs synthesized from the targeted region of *Mecp2-gfp* mRNA (Fig. 1 *C* and *D*). Editing efficiency was measured by determining relative peak heights at the targeted A position. All three *Mecp2* mutations were edited in a guide-dependent manner, consistent with ADAR2-mediated editing requiring double-stranded RNA (Fig. 1 *C* and *D*). The percent editing for a targeted A varied with the 5′ nucleotide context, similar to the sequence preference of the ADAR2 catalytic domain determined in previous studies (58, 59). Specifically, based on in vitro screens, the optimal 5′ nucleotide hierarchy for A deamination by ADAR2 catalytic domain is U > A> C > G and the most optimal 3′ nucleotides are C ~ G ~ A > U. W104X (**UAG**) was edited most efficiently (76 ± 10%), followed by R306H (**CAC,** 34 ± 3%) and R106Q (**CAA,** 25 ± 2%), which for *Mecp2* were not statistically different (Fig. 1*D*). To further optimize the Editase system for repairing *Mecp2* G > A mutations, we focused on R106Q because in human patients it is more common than the W104X mutation and leads to a more severe form of RTT than R306H (32, 60).

A Mutation in the Deaminase Domain, E488Q, Increases Editing Efficiency of the Hybrid Editase. Previous studies have reported that hADAR2 catalytic domains containing an E488Q mutation increase A > I editing efficiency by increasing both the catalytic rate (51, 61) and the affinity of the catalytic domain for substrate RNAs (59). This feature allows the E488Q mutation to achieve higher editing levels of unfavorable 5′ and 3′ contexts (51, 61). To test whether $Editase^{E488Q}$ would increase the editing efficiency of the target A in $Mecp2^{R106Q}$, which has a suboptimal 5′ C, we cotransfected N2A cells with $Mecp2^{R106Q}$-*egfp* and $Editase^{E488Q}$ cDNAs. Sequence analysis indicated that guide expression was required for editing and that the percent editing of *Mecp2* mRNA was increased ~twofold with $Editase^{E488Q}$ compared with wild-type Editase (51 ± 11% vs. 22 ± 5%, $n = 3$, $P < 0.01$) (Fig. 2*A*).

Using either wild-type hADAR2 or $hADAR2^{E488Q}$ catalytic domains in the hybrid Editase, we detected one off-target editing site within the guide region of transfected $Mecp2^{R106Q}$-*egfp* cDNA (Fig. 2*B*). Editing at this site results in a silent codon change, T105T (ACA > ACG). Previous studies indicated that a G mismatch at the off-target site reduced off-target editing in transfected substrates (49). To determine whether a G mismatch would also reduce off-target editing in *Mecp2* mRNA, we analyzed editing efficiency in N2A cells transfected with plasmids coding for $Mecp2^{R106Q}$-*egfp* cDNA, $Editase^{E488Q}$, and a guide with a G mismatch at the nearby off-target A (Fig. 2*C*). The amount of off-target editing was reduced significantly when the Editase was targeted with a guide containing the A–G mismatch (4.9 ± 0% with mismatch, 33 ± 5% without mismatch, $n = 3$, $P < 0.0001$; Fig. 2 *D* and *E*), with no significant effect on editing at the target A (Fig. 2 *D* and *F*). All of the editing events required the presence of the guide RNA (Fig. 2 *E* and *F*).

Site-Directed RNA Editing Repairs an Endogenous Rett-Causing Mutation, Restoring Protein Levels and MeCP2 Function. Next, we tested whether $Editase^{E488Q}$ could (*i*) repair the R106Q missense mutation in the endogenous *Mecp2* mRNA, (*ii*) recover protein levels, and (*iii*) restore the ability of MeCP2 to bind to heterochromatin, a hallmark functional feature required to reverse Rett-like symptoms in mice (24). For these tests, we isolated neurons from mice engineered to contain the R106Q mutation in the endogenous *Mecp2* gene (genotyping data in Fig. S1). The cultured neurons were transduced with either of two AAVs (AAV1/2). Both viruses expressed $Editase^{E488Q}$ under control of the human *Synapsin I* promoter (62), and one virus additionally contained six copies of the guide (off-target mismatch guide; Fig. 2*C*) each under control of the human U6 promoter. The other virus served as a control and lacked all guide sequences.

Hippocampal neurons were generated from P0 $Mecp2^{R106Q/y}$ mice and transduced with either guide-containing or control AAV vectors carrying the AAV1/2 hybrid capsids at 7 d in vitro

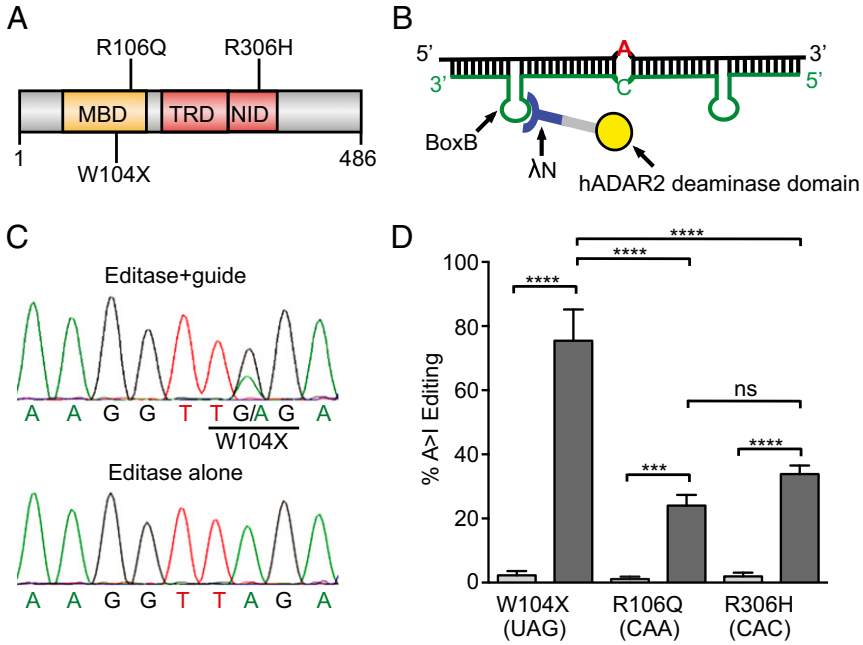

Fig. 1. Editing efficiency is sequence-dependent. (*A*) Schematic showing positions of three G > A mutations relative to the MBD, Transcriptional Repressor Domain (TRD), and NID in MeCP2. (*B*) Core components of site-directed RNA editing. The hybrid Editase contains an RNA binding domain from bacteriophage λ (λN) and the catalytic domain of hADAR2 (deaminase domain). Also included, but not shown, are three copies of an NLS and two copies of an HA-epitope tag. The guide RNA (green) is complementary to *Mecp2* mRNA (black) and contains the hairpin (stem loop) recognized by the λN RNA binding domain. In opposition to the target A (red), a C has been introduced into the guide to increase editing efficiency. (*C*) Sequencing chromatograms of *Mecp2*^{W104X} cDNA after transfection into N2A neuroblastoma cells of Editase with (*Top*) or without (*Bottom*) guide. (*D*) Percent A-to-I editing (mean ± SD; $n = 3$) quantified using direct sequencing of *Mecp2* cDNA and including data in *C*. Light-gray bars, cells transfected with Editase alone; dark-gray bars, cells transfected with Editase and guide. ***$P < 0.001$, ****$P < 0.0001$ by one-way ANOVA with Bonferroni post hoc test. ns, not significant.

(DIV 7). After allowing expression of the virus for an additional 7 d, *Mecp2* cDNA was prepared from experimental and control cultures and analyzed by Sanger sequencing. We found that 72 ± 5% of the *Mecp2* mRNA was repaired in the cultures expressing both Editase and guide (Fig. 3*A*), while there was no detectable editing in neurons transduced with the control virus that lacked guide. In addition to editing at R106Q, sequence analysis also identified several off-target editing sites within the *Mecp2* cDNA (Fig. 3*B*). The off-target sites occurred primarily within the region complementary to the guide RNA, although one event occurred outside the guide (N126S).

We first tested the functional consequences of the RNA editing by measuring the amount of MeCP2 protein in the AAV1/2 transduced cultures by Western blotting. Similar to other mutations in the MBD (63, 64), MeCP2^{R106Q} protein levels are decreased compared with wild-type levels (Fig. 4). The reduced levels of mutant MeCP2 protein are likely due to destabilization (63). Expression of the Editase and guide in the mutant primary neurons increased MeCP2 protein levels by ∼threefold compared with expression of Editase alone (Fig. 4; 35.3 ± 2% with guide compared with 12.9 ± 1% without guide, $n = 3$, $P < 0.001$).

MeCP2 binds with high affinity to methyl-CpGs, both in vitro and in vivo (27, 65), a property critical to normal function. In mouse cells, mutations in the MBD of MeCP2 reduce binding to heterochromatin that contains amplified satellite sequences rich in mCG (64, 66). MeCP2^{R106Q}, an MBD mutation, also shows reduced binding to methyl-CpGs in vitro (67). To determine whether MeCP2^{R106Q} has similarly reduced binding in cells and whether editing of G > A mutant *Mecp2* RNA restores enrichment in heterochromatin, we immunolabeled nuclei in *Mecp2*$^{R106Q/y}$ neuronal cultures transduced with AAV1/2 encoding HA-tagged Editase, with or without guide as a control (Fig. 5). We used DAPI (4′, 6-diamidino-2-phenylindole), a fluorescent indicator that binds strongly to A–T-rich regions in DNA, to identify nuclei and heterochromatin. In cultures from wild-type neurons (*Mecp2*$^{+/y}$), nuclei showed classical MeCP2 enrichment in the DAPI-stained heterochromatin (foci), reflecting a functional MBD (Fig. 5*A*). In contrast, in cultures prepared from *Mecp2*$^{R106Q/y}$ siblings transduced with Editase virus that lacked guide sequences, MeCP2 immunofluorescence was distributed diffusely throughout the nucleus, as expected for a mutation in the MBD that prevents binding to DNA (63, 66) (Fig. 5*B*). The intensity of staining was also less than in wild-type nuclei, presumably reflecting the destabilized MeCP2 protein. In contrast, *Mecp2*^{R106Q} neurons expressing both Editase and guide RNA showed a clear increase in MeCP2 immunofluorescence, to a level similar to wild-type nuclei, and enrichment of MeCP2 protein at heterochromatic foci, indicating functional restoration of the MBD (Fig. 5 *C* and *D*). To quantify the immunofluorescence results, we first determined in three experiments that Editase was expressed in the same percentage of cells irrespective of the presence of guide (Editase alone 67 ± 7%, Editase and guide 67 ± 10%; $n = 134$ and 137 cells, respectively; Fig. 5*E*). We then determined that in the cultures transduced with Editase and guide, 74 ± 11% of the cells expressing Editase (Fig. 5*F*) and 49 ± 8% of the total cells showed MeCP2 enrichment in heterochromatic foci (Fig. 5*G*). We never detected enrichment of MeCP2 within heterochromatic foci in *Mecp2*^{R106Q} nuclei transduced with virus lacking guide, consistent with our sequencing results showing that editing depended upon the presence of guide.

Discussion

The idea to use ADAR to repair G > A mutations in exogenous mRNAs was first proposed 20 y ago in experiments using *Xenopus* oocytes (68). Many iterations of this approach have been tested recently, but our study demonstrates that site-directed RNA editing, using an engineered hADAR2 catalytic domain,

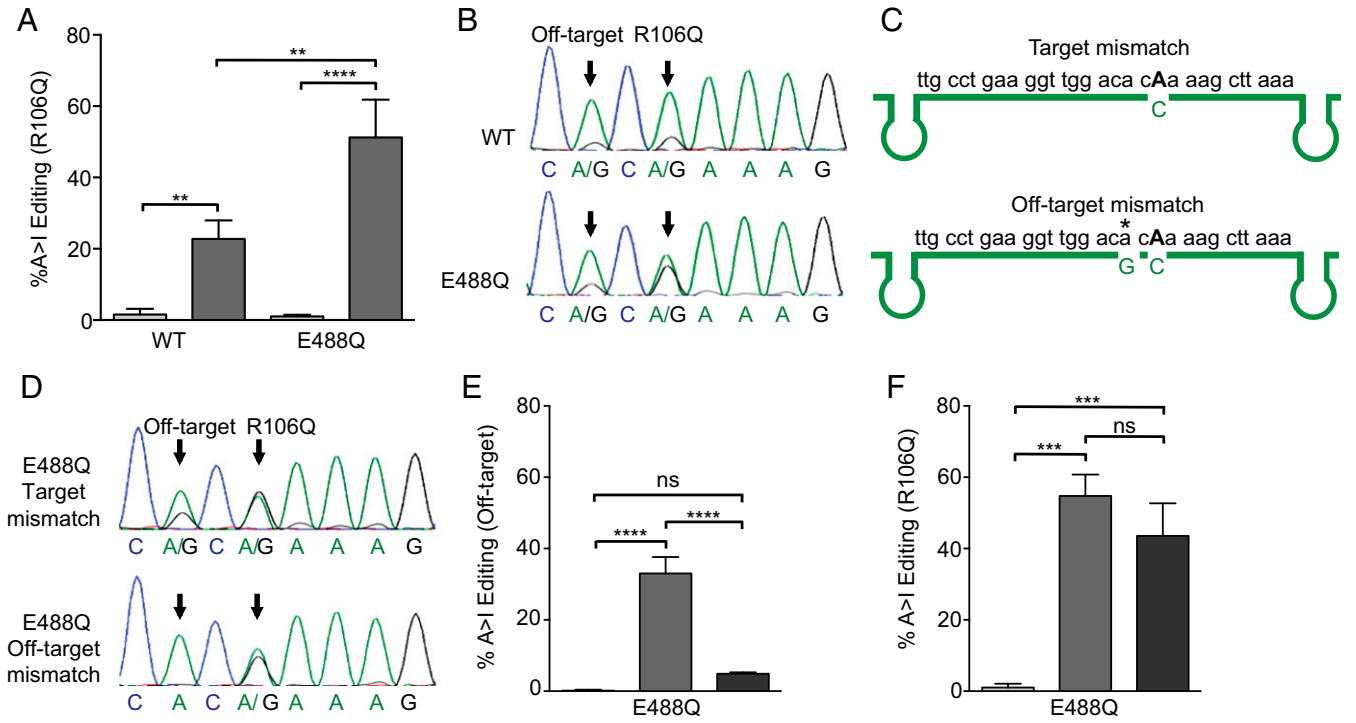

Fig. 2. Off-target editing with a more efficient Editase can be reduced using a guide with a site-specific A–G mismatch to Mecp2 mRNA. (*A*) Percent A-to-I editing at the R106Q (mean ± SD, $n = 3$) site after transfection into N2A cells of guide RNA and Editase^{WT} or Editase^{E488Q} (mean ± SD; $n = 3$, includes data in *B*). (*B*) Representative chromatograms of *Mecp2*^{R106Q} cDNA edited with Editase^{WT} (*Top*) or Editase^{E488Q} (*Bottom*). (*C*) *Mecp2* mRNA relative to two different guide RNAs (green). The standard guide (*Top*) contains an A–C mismatch (R106Q) at the target A (highlighted in bold) to enhance editing. The modified guide (*Bottom*) contains an A–G mismatch at an off-target A marked by an asterisk to inhibit editing at this site. (*D*) Chromatograms of *Mecp2* cDNA after transfection of N2A cells with Editase^{E488Q} and a guide containing only the mismatch at the target site (*Top*) or the modified guide containing both the on-target A–C mismatch and the A–G mismatch at the off-target site (*Bottom*). (*E*) Off-target editing is severely reduced with the guide containing the A–G mismatch (mean ± SD; $n = 3$, includes data in *D*). (*F*) Presence of the off-target A–G mismatch does not affect editing at the R106Q site (mean ± SD; $n = 3$, includes data in *D*). Light-gray bars, cells transfected with Editase alone; dark-gray bars, cells transfected with Editase and guide; black bars, cells transfected with Editase and guide containing the A–G mismatch. $^{**}P < 0.01$, $^{***}P < 0.001$, $^{****}P < 0.0001$ by one-way ANOVA with Bonferroni post hoc test. ns, not significant.

can repair an endogenous mutant mRNA and reverse a cellular defect caused by the mutation.

Three genes encode ADAR proteins in mouse and human, but only ADAR1 and ADAR2 exhibit A-to-I catalytic activity (69). Native ADAR-mediated editing is critically important for post-transcriptionally modulating protein function in the brain, first shown for ion channels and receptors (39–41) but now known to extend to many other proteins and noncoding RNAs (reviewed in refs. 70 and 71). We zeroed in on the ADAR2 catalytic domain because of precedence showing its ability to edit heterologous mRNAs (49–52, 56) and because of its well-characterized editing mechanism (61, 72). Indeed, we found increased editing efficiency of *Mecp2* mRNA when the Editase contained an E488Q mutation within the catalytic domain shown previously to increase efficiency (51, 61, 73). The elucidation of the structure of the hADAR2 catalytic domain complexed to double-stranded RNA (72) now provides a valuable resource for generating other mutations to further optimize editing efficiency and specificity for MeCP2 and other mutations (74). Different from previous work, all of our constructs included an NLS, which we hypothesize might increase editing efficiency, particularly of endogenous mRNAs, because ADARs normally edit primary transcripts within the nucleus (55).

In future studies, any off-target editing and potential interference with endogenous ADAR activity need to be quantitatively assessed. In transfected cells, the higher editing efficiency with Editase^{E488Q} at the targeted A also resulted in higher off-target editing at one site within the guide region. We were able to attenuate the single off-target editing site by using a G–A mismatch as published by others (50). In a previous study using transfected cells, sequencing of five cDNAs representing highly expressed mRNAs, other than the target mRNA, did not indicate off-target editing (51). However, and surprisingly, in our study with neurons, off-target editing sites were different between transfected and endogenous *Mecp2* mRNA. Specifically, in endogenous repaired *Mecp2* mRNA, we noted several additional off-target editing sites within, and one outside, the guide region that were absent from our *Mecp2* mRNA expressed from cDNA (Fig. 3*B*). The difference in off-target editing sites between transfected and endogenous *Mecp2* mRNAs likely reflects sequence differences that can affect RNA folding and other downstream processing events. Importantly, none of the off-target sites in the endogenous *Mecp2* mRNA are reported to cause RTT (32). However, it is essential to determine the extent of off-target editing by global transcriptomic analysis, and it will be best to perform these studies in mice where functional and physiological correlates may be accomplished at the same time. RTT mouse models are an ideal test system for assessing this important issue in the future because cellular and behavioral symptoms can be reversed by restoration of wild-type MeCP2 in symptomatic mice (21–25).

Materials and Methods

Plasmid Constructions. A pcDNA 3.1+ plasmid Thermo Fisher Scientific coding for the λN peptide fused to the wild-type ADAR2 catalytic domain (Editase) has been described previously (51, 52). The Editase^{E488Q} cDNA was generated by overlapping PCR of wild-type Editase and cloned into pcDNA3.1+. Both versions of Editase were modified in pcDNA3.1+ by inserting two copies of

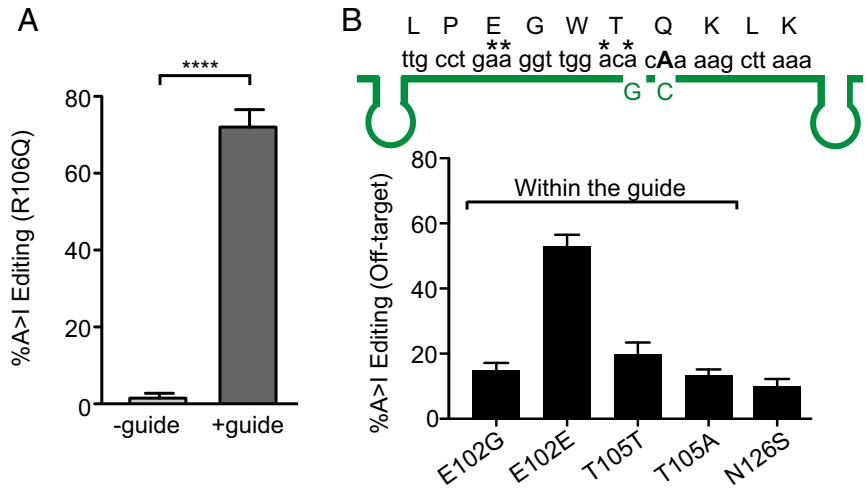

Fig. 3. Sequence analysis of endogenous MeCP2 mRNA following AAV1/2 transduction of primary neurons. (*A*) Quantification of editing (mean ± SD, $n = 3$) by sequence analysis of cDNA isolated from *Mecp2*$^{R106Q/y}$ hippocampal neurons (DIV14), 7 d following transduction with AAV1/2 virus. +guide refers to AAV1/2 that contains Editase under control of the neuronal *Synapsin I* promoter (62) and six copies of the guide, each expressed under control of a U6 promoter. The guide contains a C mismatch at the targeted A for R106Q and a G mismatch at the off-target A T105T. The control virus contains Editase under control of the *Synapsin I* promoter but lacks any guide sequences (–guide). ****$P < 0.0001$ by unpaired two-tailed *t* test. (*B*, *Top*) *Mecp2* mRNA and primary amino acid sequences relative to the guide RNA region (green). The target A is bolded, and asterisks indicate off-target edited A residues. The hairpins in the guide represent the positions of the BoxB sequences recognized by λN peptide. (*B*, *Bottom*) Quantitation of editing at the off-target sites within *Mecp2* mRNA (mean ± SD; $n = 3$). Residue N126S lies outside the guide region.

an HA epitope and three copies of the SV40 NLS in frame and N-terminal to the hybrid Editase (pGM1090, wild type; pGM1091, E488Q). Cloning details for adding the epitope and NLS are found in *SI Materials and Methods*. For *Mecp2–BoxB* guides, synthetic oligonucleotides representing the three different *Mecp2* G > A mutations, and their antisense sequences, were annealed with Bsa1 overhangs and cloned into the pENTR/U6 polylinker [pGM1099 (W104X), pGM1181 (306H), pGM1085 (R106Q)] (Thermo Fisher Scientific). The *Mecp2–BoxB* guide containing the off-target A–G mismatch (pGM11089) is also in pENTR/U6. For the *Mecp2* editing substrate, an EcoRI–KpnI fragment of mouse *Mecp2* E1 isoform cDNA (NP_001075448.1) was cloned into the multiple cloning site of pEGFP-N3 (Clontech). Individual G > A mutations of *Mecp2* were generated by overlapping PCR with the same restriction site overhangs and cloned in-frame as a fusion protein with eGFP in pEGFP-N3 (Thermo Fisher Scientific). All subcloning was verified by sequence analysis. Primer sequences used in plasmid constructions and PCR amplifications are found in *SI Materials and Methods* and Table S1.

AAV Vector and Virus Preparation. The AAV1/2 backbone vector, pX552, containing the human *Synapsin I* promoter was described previously (62) and obtained from Addgene (plasmid 60958). We modified pX552 by replacing the eGFP-KASH coding sequence with the HA-tagged NLS Editase cDNA, without and with six copies of guide cDNAs (pGM1186, Editase only; pGM1258, Editase and R106Q guides). More details on construction of pGM1186 are found in *SI Materials and Methods*. Editase and guide sequences were verified by sequence analysis before generating virus.

Each AAV1/2 chimeric vector was produced in human embryonic kidney 293 (HEK293) cells on a scale of three 225 cm^2 flasks per vector by an adenovirus-free plasmid transfection method (75, 76). In each flask, ~2×10^7 HEK293 cells were transfected with a total of 45 μg of the following four plasmid DNAs mixed with polyethyleneimine (PEI) at a DNA:PEI weight ratio of 1:2. The plasmid DNA mixture contained 15 μg of pHelper (Agilent), 7.5 μg each of pHLP19-1 and pHLP19-2, and one of the AAV vector Editase recombinant plasmids (15 μg) containing AAV vector genome sequences with two inverted terminal repeats (ITRs). pHLP19-1 is an AAV1 helper plasmid supplying AAV2 Rep proteins and AAV1 VP proteins, and pHLP19-2 is an AAV2 helper plasmid supplying AAV2 Rep proteins and AAV2 VP proteins (77). Three days posttransfection, cells were harvested. AAV vector particles were then recovered from the cells by cell lysis and purified using HiTrap heparin column (GE Healthcare), as described in ref. 55. The titer of each virus was determined by a quantitative dot blot assay using a probe generated against the Editase coding sequence.

Cell Culture. Neuro2A cells (ATCC CCL-131) were maintained in DMEM (Thermo Fisher Technologies) in 10% FBS (lot no. AAC20-0955; HyClone) at 37 °C in 5% CO_2 humidified incubator. Primary neurons were derived from the *Mecp2*^{R106Q} mouse line that was generated by targeted homologous recombination (Janelia Farms) and characterized by genotyping (Fig. S1). All animal studies were approved by the Oregon Health and Science University Institutional Animal Care and Use Committee. Pups (P0) were killed by decapitation and the brains dissected in ice-cold Hanks Basal Salt Solution (HBSS, pH 7.4) with 25 mM Hepes. Individual hippocampi were excised without the meninges and pooled by genotype. The tissue was treated with 1% trypsin and 0.01% DNase I in HBSS at 37 °C for 10 min. Tissue pieces were rinsed three times at room temperature in HBSS and dissociated in Minimal Essential Media (Gibco) containing 25 mM glucose, 1% penn/strep, 1% horse serum (lot no. B02307-7021; HyClone), and 1% FBS. Neurons were dissociated by filtering through a 0.4-μm filter and plated in poly-L-lysine–coated dishes at a density of 5×10^5 cells per well in a 12-well dish or 5×10^4 in a 96-well glass chamber, in neuronal growth media consisting of Neurobasal-A (Thermo Fisher Scientific), 1× Glutamax (Thermo Fisher Scientific), 2% B27 (Thermo Fisher Scientific), and penn/strep. After 24 h, neurons received a full

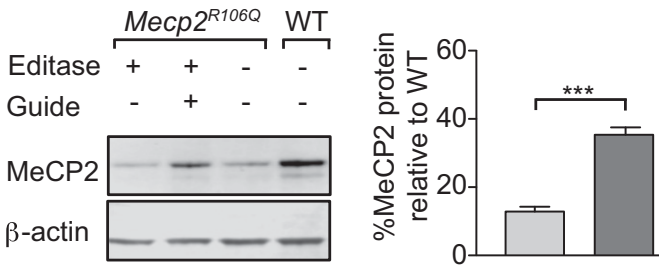

Fig. 4. Site-directed RNA editing increases MeCP2 protein levels. (*Top*) Representative Western blot of whole-cell lysates from *Mecp2*$^{R106Q/y}$ or wild-type (WT, *Mecp2*$^{+/y}$) sibling hippocampal neurons (DIV14) transduced 7 d earlier with AAV1/2 expressing either Editase alone or Editase and guide. The guide contains a C mismatch at the R106Q site and a G mismatch at the off-target A, T105T. (*Bottom*) Quantification of Western blots (mean ± SD, $n = 3$), each condition normalized to β-actin. Light-gray bar, cells transduced with Editase alone; dark-gray bar, cells transduced with Editase and guide. ***$P < 0.001$ by unpaired two-tailed *t* test.

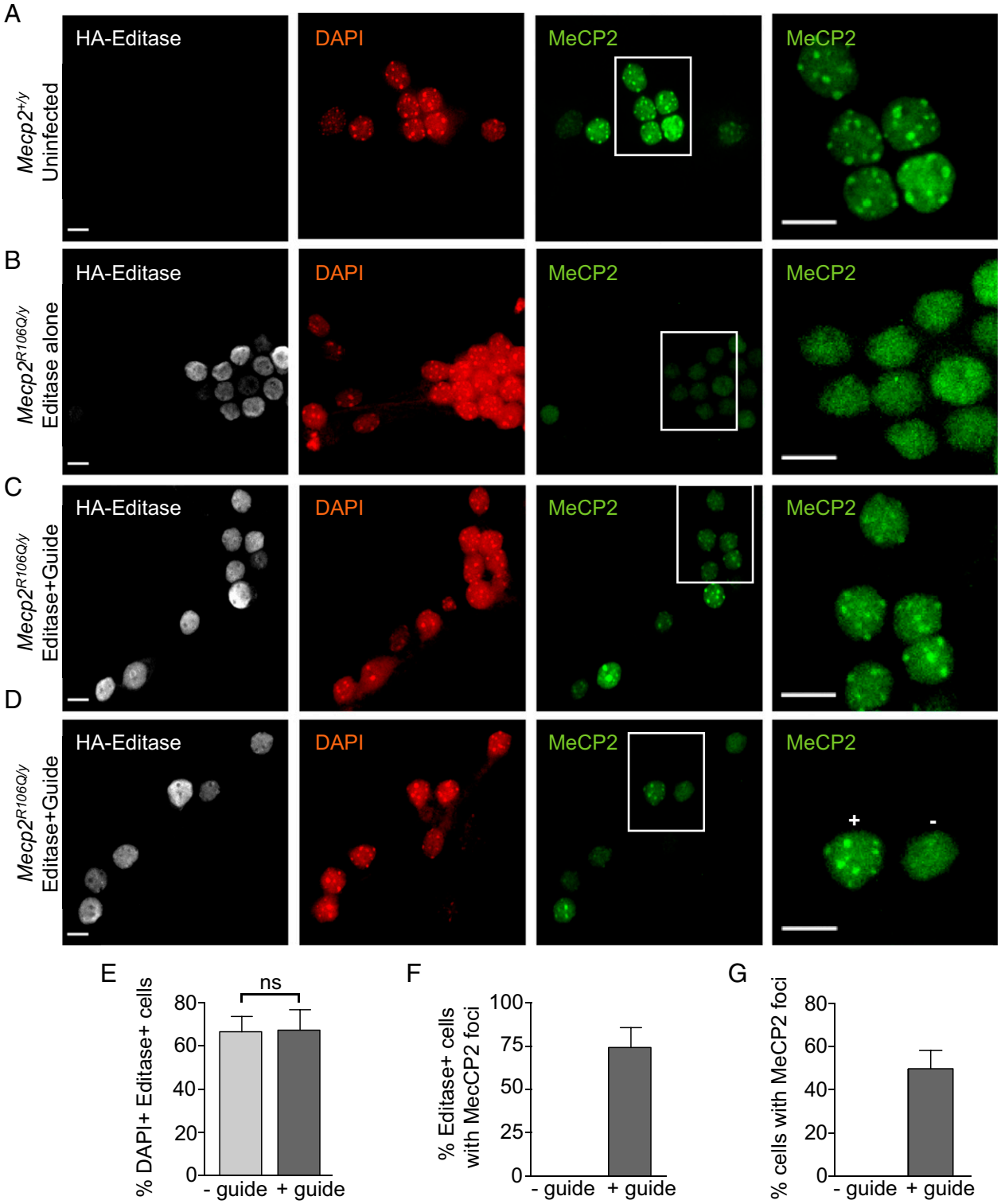

Fig. 5. Site-directed RNA editing restores the ability of MeCP2 to bind to heterochromatin. Shown are representative confocal images of hippocampal neurons (DIV14) immunolabeled for Editase (HA) and MeCP2. DAPI staining outlines the nuclei and shows heterochromatic foci. *Insets* demarcate the cells imaged at higher magnification and higher gain in the adjacent panels. (*A*) Wild-type (*Mecp2*$^{+/y}$) neuronal cultures. (*B*) *Mecp2*$^{R106Q/y}$ neuronal cultures transduced with AAV1/2 virus expressing Editase alone (no guide). These neurons never exhibited MeCP2 enrichment in heterochromatin. (*C* and *D*) *Mecp2*$^{R106Q/y}$ neuronal cultures transduced with AAV1/2 virus expressing Editase and guide containing the C mismatch at the target A. In *D*, + and − indicate nuclei with the presence and absence, respectively, of MeCP2 enrichment in heterochromatin. While there appears to be a relationship between Editase/guide expression and MeCP2 heterochromatic enrichment in this image, overall we were not able to confidently support this relationship. (Scale bar, 10 μm.) (*E* and *G*) Each histogram represents quantification of cells (Editase alone, $n = 134$; Editase and guide, $n = 137$) from three fields in each of three slides (mean ± SD). (*E*) Percentage of Editase+ cells identified by HA nuclear staining after thresholding signals from uninfected cells. Percentages are relative to the total number of DAPI+ cells. (*F*) Percentage of Editase+ cells with MeCP2 enrichment in heterochromatin (foci) and (*G*) percentage of all cells with MeCP2 enrichment in heterochromatin (foci). ns, not significant.

medium change to remove cellular debris. Half medium changes were done every 2–3 d. Cells were maintained at 37 °C in 5% CO_2.

RNA Editing. For analysis of N2A cells, cells were seeded at a density of 1.3×10^3 cells per well in a 12-well plate. After 24 h, cells were transfected with plasmids containing wild-type or E488Q Editase (pGM1090 and 1091), one copy of guide (pGM1099, pGM1181 or pGM1108), and *Mecp2-egfp* cDNAs (pGM1174, pGM1172, or pGM1173) using a 2:1 ratio of Lipofectamine 2000 (Thermo Fisher Scientific) and DNA in Opti-MEM reduced serum media (Thermo Fisher Scientific). The amount of plasmid DNA added per well was 125 ng target, 250 ng Editase, and 2.5 μg guide. After 72 h, cells were harvested and total RNA was isolated using the Purelink RNA Mini kit (Ambion) according to the manufacturer's instructions. Residual plasmid DNA was removed using the TURBO DNA-free kit (Ambion). Total RNA was reverse transcribed using the SuperScript III First-Strand Synthesis System (Life Technologies) and primed using oligo dT. The transfected *Mecp2-egfp* cDNAs were amplified for sequence analysis by PCR using a 5′ primer in the CMV promoter in pEGFP-N3 and a reverse primer in the *egfp* gene. For editing analysis of primary neurons, at DIV7, 5×10^5 hippocampal primary neurons were transduced with AAV1/2 at a multiplicity of infection of $3–6 \times 10^4$ viral genomes per cell. Viral volume did not exceed 5% of total medium volume. Cells were harvested 1-wk posttransduction and analyzed for editing efficiency as described for the transfected N2A cells.

The efficiency of A to I editing was determined by reverse transcription PCR (RT-PCR) and direct sequencing of PCR products. Quantification of the sequencing peak heights from the antisense strand was determined by processing the four-dye-trace sequences using the Bioedit Software package (www.mbio.ncsu.edu/BioEdit/bioedit.html; File > Batch Export of Raw Sequence Trace Data). The amount of editing at each site was then determined using the maximum height of the T (nonedited) and C (edited) peaks at a given site and calculating the percentage of cDNA edited {100% × [C height/(T height + C height)]}. A detection limit of 5% editing was determined by measuring G–A peak heights in mixtures containing decreasing ratios of R106Q mutant to wild-type Mecp2 plasmids. The C/T peak heights of the antisense strand was quantified because it is more accurate than using the A/G peak heights of the sense strand (58), however for clarity all chromatograms are shown in the reverse complement.

Western Blotting. Primary hippocampal neurons, transduced with AAV1/2, were lysed in 100 μL of whole-cell lysis buffer (25 mM Tris, pH 7.6, 150 mM NaCl, 1% Igepal CA-630; Sigma), 1% deoxycholate, 0.1% SDS, protease inhibitor (Complete EDTA-free; Roche), 1 mM beta-mercaptoethanol, and 250 units per mL benzonase (Sigma-Aldrich). Lysates were centrifuged at 9,300 × *g* for 10 min at 4 °C and the soluble fraction isolated. Protein concentrations were measured using the BCA protein assay kit (Pierce Biotechnology). Equal amounts of protein lysates were separated on NuPage 4–12% Bis–Tris gels (Thermo Fisher Scientific) in Mops-SDS running buffer (Thermo Fisher Scientific), and proteins were blotted onto a nitrocellulose membrane (GE Healthcare Life Sciences). Membranes were blocked with 3% BSA in 1× TBST (TBS with 0.05% Tween 20) for 1 h, then incubated with either rabbit anti-mMeCP2 (Covance) or rabbit anti–β-actin (8227; Abcam) overnight at 4 °C. After washing three times with 1× TBST, blots were incubated with anti-rabbit IgG DyLight 680 (1:10,000 dilution; Thermo Scientific) for 1 h. Blots were quantified using the Odyssey Imaging System (LI-COR Biosciences).

Immunostaining. Hippocampal primary neurons were fixed in 4% paraformaldehyde in PBS for 20 min at room temperature. Fixed cells were washed twice with 1× PBSG (0.1 M glycine in 1× PBS) at room temperature for 10 min. Then, cells were blocked and permeabilized [0.5% Igepal CA-630, Sigma; 3% BSA (source) in 1× PBS] for 1 h at 4 °C and incubated with primary antibodies raised against MeCP2 (rabbit mAb D4F3; Cell Signaling) and HA (rat mAb 3F10; Roche) in a humidified chamber overnight at 4 °C. Cells were washed three times in 1× PBS containing 0.5% Igepal and incubated with secondary antibodies Alexa 488 and Alexa 568 (Thermo Fisher Scientific) for 1 h. After another wash with 1× PBS containing 0.5% Igepal, cells were incubated with 300 nM DAPI for 5 min, then washed again with 1× PBS. The cells were mounted using ProLong Gold antifade reagent (Thermo Fisher Scientific) overnight. All images were acquired as *z*-stacks of 0.5-μm optical sections on a Zeiss 710 confocal microscope using a 40× water immersion objective. HA and MeCP2 fluorescent images were taken using the same settings across all samples. Total cell number or numbers of antibody-positive cells were determined by ImageJ cell counter plugin [National Institutes of Health, https://imagej.nih.gov/ij, version 1.60_65 (32 bit)].

Statistical Analysis. All statistics were performed using GraphPad version 6.0 software (Prism). The percentage of A to I editing in N2A cells was analyzed using one-way ANOVA followed by Bonferroni post hoc tests. The level of A to I editing in *Mecp2*$^{R106Q/y}$ transduced neurons, Western blots comparing MeCP2 protein levels, and the number of neurons showing MeCP2 enrichment at heterochromatic foci were each analyzed using unpaired *t* tests. All experimental results are expressed as mean ± SD.

ACKNOWLEDGMENTS. We thank Drs. Maria Montiel-Gonzalez and Joshua Rosenthal (Marine Biological Laboratories) for kindly providing the initial Editase construct and for useful discussions. We also thank Dr. Paul Brehm (Vollum Institute, OHSU) and members of the G.M. laboratory for advice during the course of the work and Ms. Christine Schmidt (Vollum Institute, OHSU) for excellent technical support. We acknowledge the laboratories of Drs. Michael E. Greenberg (Harvard Medical School) and Adrian Bird (Wellcome Trust Centre for Cell Biology, University of Edinburgh) for advice and encouragement through the Rett Syndrome Research Trust (RSRT) Consortium. This work was supported by NIH Grants NS087726 (to G.M.) and NS088399 (to H.N.) and the Rett Syndrome Research Trust (G.M.).

1. Amir RE, et al. (1999) Rett syndrome is caused by mutations in X-linked MECP2, encoding methyl-CpG-binding protein 2. *Nat Genet* 23:185–188.
2. Neul JL, et al.; RettSearch Consortium (2010) Rett syndrome: Revised diagnostic criteria and nomenclature. *Ann Neurol* 68:944–950.
3. Percy AK, et al. (2010) Rett syndrome diagnostic criteria: Lessons from the natural history study. *Ann Neurol* 68:951–955.
4. Schüle B, Armstrong DD, Vogel H, Oviedo A, Francke U (2008) Severe congenital encephalopathy caused by MECP2 null mutations in males: Central hypoxia and reduced neuronal dendritic structure. *Clin Genet* 74:116–126.
5. Guy J, Hendrich B, Holmes M, Martin JE, Bird A (2001) A mouse Mecp2-null mutation causes neurological symptoms that mimic Rett syndrome. *Nat Genet* 27:322–326.
6. Lioy DT, et al. (2011) A role for glia in the progression of Rett's syndrome. *Nature* 475:497–500.
7. Chen RZ, Akbarian S, Tudor M, Jaenisch R (2001) Deficiency of methyl-CpG binding protein-2 in CNS neurons results in a Rett-like phenotype in mice. *Nat Genet* 27:327–331.
8. Luikenhuis S, Giacometti E, Beard CF, Jaenisch R (2004) Expression of MeCP2 in postmitotic neurons rescues Rett syndrome in mice. *Proc Natl Acad Sci USA* 101:6033–6038.
9. Ross PD, et al. (2016) Exclusive expression of MeCP2 in the nervous system distinguishes between brain and peripheral Rett syndrome-like phenotypes. *Hum Mol Genet* 25:4389–4404.
10. Belichenko NP, Belichenko PV, Mobley WC (2009) Evidence for both neuronal cell autonomous and nonautonomous effects of methyl-CpG-binding protein 2 in the cerebral cortex of female mice with Mecp2 mutation. *Neurobiol Dis* 34:71–77.
11. Belichenko PV, et al. (2009) Widespread changes in dendritic and axonal morphology in Mecp2-mutant mouse models of Rett syndrome: Evidence for disruption of neuronal networks. *J Comp Neurol* 514:240–258.
12. Fukuda T, Itoh M, Ichikawa T, Washiyama K, Goto Y (2005) Delayed maturation of neuronal architecture and synaptogenesis in cerebral cortex of Mecp2-deficient mice. *J Neuropathol Exp Neurol* 64:537–544.
13. Kishi N, Macklis JD (2004) MECP2 is progressively expressed in post-migratory neurons and is involved in neuronal maturation rather than cell fate decisions. *Mol Cell Neurosci* 27:306–321.
14. Robinson L, et al. (2012) Morphological and functional reversal of phenotypes in a mouse model of Rett syndrome. *Brain* 135:2699–2710.
15. Tropea D, et al. (2009) Partial reversal of Rett syndrome-like symptoms in MeCP2 mutant mice. *Proc Natl Acad Sci USA* 106:2029–2034.
16. Stuss DP, Boyd JD, Levin DB, Delaney KR (2012) MeCP2 mutation results in compartment-specific reductions in dendritic branching and spine density in layer 5 motor cortical neurons of YFP-H mice. *PLoS One* 7:e31896.
17. Armstrong D, Dunn JK, Antalffy B, Trivedi R (1995) Selective dendritic alterations in the cortex of Rett syndrome. *J Neuropathol Exp Neurol* 54:195–201.
18. Li Y, et al. (2013) Global transcriptional and translational repression in human-embryonic-stem-cell-derived Rett syndrome neurons. *Cell Stem Cell* 13:446–458.
19. Belichenko PV, Oldfors A, Hagberg B, Dahlström A (1994) Rett syndrome: 3-D confocal microscopy of cortical pyramidal dendrites and afferents. *Neuroreport* 5:1509–1513.
20. Bauman ML, Kemper TL, Arin DM (1995) Pervasive neuroanatomic abnormalities of the brain in three cases of Rett's syndrome. *Neurology* 45:1581–1586.
21. Guy J, Gan J, Selfridge J, Cobb S, Bird A (2007) Reversal of neurological defects in a mouse model of Rett syndrome. *Science* 315:1143–1147.
22. Sinnett SE, et al. (2017) Improved MECP2 gene therapy extends the survival of MeCP2-null mice without apparent toxicity after intracisternal delivery. *Mol Ther Methods Clin Dev* 5:106–115.
23. Gadalla KKE, et al. (2017) Development of a novel AAV gene therapy cassette with improved safety features and efficacy in a mouse model of Rett syndrome. *Mol Ther Methods Clin Dev* 5:180–190.

24. Garg SK, et al. (2013) Systemic delivery of MeCP2 rescues behavioral and cellular deficits in female mouse models of Rett syndrome. *J Neurosci* 33:13612–13620.
25. Gadalla KK, et al. (2013) Improved survival and reduced phenotypic severity following AAV9/MECP2 gene transfer to neonatal and juvenile male Mecp2 knockout mice. *Mol Ther* 21:18–30.
26. Van Esch H, et al. (2005) Duplication of the MECP2 region is a frequent cause of severe mental retardation and progressive neurological symptoms in males. *Am J Hum Genet* 77:442–453.
27. Skene PJ, et al. (2010) Neuronal MeCP2 is expressed at near histone-octamer levels and globally alters the chromatin state. *Mol Cell* 37:457–468.
28. Ballas N, Lioy DT, Grunseich C, Mandel G (2009) Non-cell autonomous influence of MeCP2-deficient glia on neuronal dendritic morphology. *Nat Neurosci* 12:311–317.
29. Shahbazian MD, Antalffy B, Armstrong DL, Zoghbi HY (2002) Insight into Rett syndrome: MeCP2 levels display tissue- and cell-specific differences and correlate with neuronal maturation. *Hum Mol Genet* 11:115–124.
30. Sugino K, et al. (2014) Cell-type-specific repression by methyl-CpG-binding protein 2 is biased toward long genes. *J Neurosci* 34:12877–12883.
31. Linhoff MW, Garg SK, Mandel G (2015) A high-resolution imaging approach to investigate chromatin architecture in complex tissues. *Cell* 163:246–255.
32. Fyfe S, Cream A, de Klerk N, Christodoulou J, Leonard H (2003) InterRett and RettBASE: International Rett syndrome association databases for Rett syndrome. *J Child Neurol* 18:709–713.
33. Bass BL, Weintraub H (1988) An unwinding activity that covalently modifies its double-stranded RNA substrate. *Cell* 55:1089–1098.
34. Bass BL, Weintraub H (1987) A developmentally regulated activity that unwinds RNA duplexes. *Cell* 48:607–613.
35. Melcher T, et al. (1996) A mammalian RNA editing enzyme. *Nature* 379:460–464.
36. O'Connell MA, Gerber A, Keegan LP (1998) Purification of native and recombinant double-stranded RNA-specific adenosine deaminases. *Methods* 15:51–62.
37. Kim U, Wang Y, Sanford T, Zeng Y, Nishikura K (1994) Molecular cloning of cDNA for double-stranded RNA adenosine deaminase, a candidate enzyme for nuclear RNA editing. *Proc Natl Acad Sci USA* 91:11457–11461.
38. Basilio C, Wahba AJ, Lengyel P, Speyer JF, Ochoa S (1962) Synthetic polynucleotides and the amino acid code. V. *Proc Natl Acad Sci USA* 48:613–616.
39. Bhalla T, Rosenthal JJ, Holmgren M, Reenan R (2004) Control of human potassium channel inactivation by editing of a small mRNA hairpin. *Nat Struct Mol Biol* 11: 950–956.
40. Sommer B, Köhler M, Sprengel R, Seeburg PH (1991) RNA editing in brain controls a determinant of ion flow in glutamate-gated channels. *Cell* 67:11–19.
41. Burns CM, et al. (1997) Regulation of serotonin-2C receptor G-protein coupling by RNA editing. *Nature* 387:303–308.
42. Dawson TR, Sansam CL, Emeson RB (2004) Structure and sequence determinants required for the RNA editing of ADAR2 substrates. *J Biol Chem* 279:4941–4951.
43. Higuchi M, et al. (1993) RNA editing of AMPA receptor subunit GluR-B: A base-paired intron-exon structure determines position and efficiency. *Cell* 75:1361–1370.
44. Maas S, et al. (1996) Structural requirements for RNA editing in glutamate receptor pre-mRNAs by recombinant double-stranded RNA adenosine deaminase. *J Biol Chem* 271:12221–12226.
45. Lomeli H, et al. (1994) Control of kinetic properties of AMPA receptor channels by nuclear RNA editing. *Science* 266:1709–1713.
46. Yang JH, Sklar P, Axel R, Maniatis T (1997) Purification and characterization of a human RNA adenosine deaminase for glutamate receptor B pre-mRNA editing. *Proc Natl Acad Sci USA* 94:4354–4359.
47. Hanswillemenke A, Kuzdere T, Vogel P, Jékely G, Stafforst T (2015) Site-directed RNA editing in vivo can be triggered by the light-driven assembly of an artificial riboprotein. *J Am Chem Soc* 137:15875–15881.
48. Vogel P, Stafforst T (2014) Site-directed RNA editing with antagomir deaminases–A tool to study protein and RNA function. *ChemMedChem* 9:2021–2025.
49. Vogel P, Schneider MF, Wettengel J, Stafforst T (2014) Improving site-directed RNA editing in vitro and in cell culture by chemical modification of the guideRNA. *Angew Chem Int Ed Engl* 53:6267–6271.
50. Schneider MF, Wettengel J, Hoffmann PC, Stafforst T (2014) Optimal guideRNAs for re-directing deaminase activity of hADAR1 and hADAR2 in trans. *Nucleic Acids Res* 42: e87.
51. Montiel-González MF, Vallecillo-Viejo IC, Rosenthal JJ (2016) An efficient system for selectively altering genetic information within mRNAs. *Nucleic Acids Res* 44:e157.
52. Montiel-Gonzalez MF, Vallecillo-Viejo I, Yudowski GA, Rosenthal JJ (2013) Correction of mutations within the cystic fibrosis transmembrane conductance regulator by site-directed RNA editing. *Proc Natl Acad Sci USA* 110:18285–18290.
53. Austin RJ, Xia T, Ren J, Takahashi TT, Roberts RW (2002) Designed arginine-rich RNA-binding peptides with picomolar affinity. *J Am Chem Soc* 124:10966–10967.
54. Lyst MJ, et al. (2013) Rett syndrome mutations abolish the interaction of MeCP2 with the NCoR/SMRT co-repressor. *Nat Neurosci* 16:898–902.
55. Desterro JM, et al. (2003) Dynamic association of RNA-editing enzymes with the nucleolus. *J Cell Sci* 116:1805–1818.
56. Wong SK, Sato S, Lazinski DW (2001) Substrate recognition by ADAR1 and ADAR2. *RNA* 7:846–858.
57. Källman AM, Sahlin M, Ohman M (2003) ADAR2 A–>I editing: Site selectivity and editing efficiency are separate events. *Nucleic Acids Res* 31:4874–4881.
58. Eggington JM, Greene T, Bass BL (2011) Predicting sites of ADAR editing in double-stranded RNA. *Nat Commun* 2:319.
59. Lehmann KA, Bass BL (2000) Double-stranded RNA adenosine deaminases ADAR1 and ADAR2 have overlapping specificities. *Biochemistry* 39:12875–12884.
60. Cuddapah VA, et al. (2014) Methyl-CpG-binding protein 2 (MECP2) mutation type is associated with disease severity in Rett syndrome. *J Med Genet* 51:152–158.
61. Kuttan A, Bass BL (2012) Mechanistic insights into editing-site specificity of ADARs. *Proc Natl Acad Sci USA* 109:E3295–E3304.
62. Swiech L, et al. (2015) In vivo interrogation of gene function in the mammalian brain using CRISPR-Cas9. *Nat Biotechnol* 33:102–106.
63. Goffin D, et al. (2011) Rett syndrome mutation MeCP2 T158A disrupts DNA binding, protein stability and ERP responses. *Nat Neurosci* 15:274–283.
64. Brown K, et al. (2016) The molecular basis of variable phenotypic severity among common missense mutations causing Rett syndrome. *Hum Mol Genet* 25:558–570.
65. Lagger S, et al. (2017) MeCP2 recognizes cytosine methylated tri-nucleotide and di-nucleotide sequences to tune transcription in the mammalian brain. *PLoS Genet* 13: e1006793.
66. Heckman LD, Chahrour MH, Zoghbi HY (2014) Rett-causing mutations reveal two domains critical for MeCP2 function and for toxicity in MECP2 duplication syndrome mice. *eLife* 3:e02676.
67. Yang Y, Kucukkal TG, Li J, Alexov E, Cao W (2016) Binding analysis of methyl-CpG binding domain of MeCP2 and Rett syndrome mutations. *ACS Chem Biol* 11: 2706–2715.
68. Woolf TM, Chase JM, Stinchcomb DT (1995) Toward the therapeutic editing of mutated RNA sequences. *Proc Natl Acad Sci USA* 92:8298–8302.
69. Nishikura K (2010) Functions and regulation of RNA editing by ADAR deaminases. *Annu Rev Biochem* 79:321–349.
70. Chen LL, Carmichael GG (2012) Nuclear editing of mRNA 3′-UTRs. *Curr Top Microbiol Immunol* 353:111–121.
71. Nishikura K (2016) A-to-I editing of coding and non-coding RNAs by ADARs. *Nat Rev Mol Cell Biol* 17:83–96.
72. Matthews MM, et al. (2016) Structures of human ADAR2 bound to dsRNA reveal base-flipping mechanism and basis for site selectivity. *Nat Struct Mol Biol* 23:426–433.
73. Phelps KJ, et al. (2015) Recognition of duplex RNA by the deaminase domain of the RNA editing enzyme ADAR2. *Nucleic Acids Res* 43:1123–1132.
74. Wang Y, Beal PA (2016) Probing RNA recognition by human ADAR2 using a high-throughput mutagenesis method. *Nucleic Acids Res* 44:9872–9880.
75. Matsushita T, et al. (1998) Adeno-associated virus vectors can be efficiently produced without helper virus. *Gene Ther* 5:938–945.
76. Earley LF, et al. (2017) Adeno-associated virus (AAV) assembly-activating protein is not an essential requirement for capsid assembly of AAV serotypes 4, 5, and 11. *J Virol* 91:e01980-16.
77. Grimm D, et al. (2003) Preclinical in vivo evaluation of pseudotyped adeno-associated virus vectors for liver gene therapy. *Blood* 102:2412–2419.